

Strong gravitational lensing by Kerr and Kerr-Newman black holes

Tien Hsieh, Da-Shin Lee,^{*} and Chi-Yong Lin[†]

*Department of Physics, National Dong Hwa University,
Hualien 97401, Taiwan, Republic of China*

(Dated: December 13, 2023)

Abstract

We study the strong gravitational lensing due to the Kerr black holes with angular momentum a and the Kerr-Newman black holes with additional charge Q . We first derive the analytical expressions of the deflection angles of light rays that particularly diverge as they travel near the photon sphere. In this strong deflection limit, the light rays can circle around the black hole multiple times before reaching the observer, giving relativistic images. The obtained analytical expressions are then applied to compute the angular positions and the magnifications of relativistic images due to the supermassive galactic black holes. In this work, we focus on the outermost image with reference to the optical axis. We find that its angular separation from the one closest to the optical axis and the magnification increase in angular momentum a of the black holes for light rays with direct orbits. Additionally, the effects of the charge Q of black holes also increase the angular separation of the outermost image from the others and the magnification for both direct and retrograde orbits. The potentially increasing observability of the relativistic images from the effects of angular momentum and charge of the black holes will be discussed.

PACS numbers: 04.70.-s, 04.70.Bw, 04.80.Cc

^{*}Electronic address: dslee@gms.ndhu.edu.tw

[†]Electronic address: lyong@gms.ndhu.edu.tw

I. INTRODUCTION

Gravitational lensing is one of the powerful tools to test general relativity (GR) [1, 2]. Weak lensing has been fully studied in the formalism of weak field approximations, with which to successfully explain various lensing phenomena in a broad array of astrophysical contexts [3]. Nevertheless, in recent years, there have been significant theoretical studies looking into lensing phenomena from strong field perspectives [4–15]. Through the gravitational lensing in the vicinity of the compact massive objects such as a black hole would provide another avenue to test GR. So far, observational evidence has shown that almost every large galaxy has a supermassive black hole at the galaxy’s center [16]. The Milky Way has a supermassive black hole in its Galactic Center with the location of Sagittarius A* [17, 18]. Together with the first image of the black hole captured by the Event Horizon Telescope [19–21], gravitational lensing will also become an important probe to study the isolated dim black hole.

Recently, Virbhadra and Ellis have developed a new gravitational lens equation, which allows to study large deflection of light rays, resulting in the strong gravitational lensing [4]. This lens equation is then applied to analyze the lensing by a Schwarzschild black hole in the center of the galaxy using numerical methods. Later, Frittelli *et al.* propose the definition of an exact lens equation without reference to the background spacetime, and construct the exact lens equation explicitly in the Schwarzschild spacetime [5]. Strong field lensing in the general spherically symmetric and static spacetime is first studied analytically by Bozza in [6, 7, 9] and later by Tsukamoto in [12, 13]. These works have shown that the deflection angle $\hat{\alpha}(b)$ of light rays for a given impact parameter b , which in the strong deflection limit (SDL) as $b \rightarrow b_c$, can be approximated in the form

$$\hat{\alpha}(b) \approx -\bar{a} \log \left(\frac{b}{b_c} - 1 \right) + \bar{b} + O(b - b_c) \log(b - b_c) \quad (1)$$

with two parameters \bar{a} and \bar{b} as a function of the black hole’s parameters. Then, in [8], the Kerr black hole of the non-spherically symmetric black holes is considered, exploring \bar{a} and \bar{b} numerically. In this paper, we extend the works of [6] and [12, 13] and find the analytic form of \bar{a} and \bar{b} for non-spherically symmetric Kerr and Kerr-Newman black holes, respectively, using the analytical closed-form expressions of the deflection angles in [22] and [23]. Although one might not expect that astrophysical black holes to have large residue

electric charge, some accretion scenarios are proposed to investigate the possibility of the spinning charged back holes [24, 25]. It is then still of great interest to extend the previous studies to the Kerr-Newman black holes [26–28]. The analytical expressions can be applied to examine the lensing effects due to the supermassive galactic black holes on the source as illustrated in Fig.(1). The light rays are emitted from the source, and circle around the black hole multiple times in the SDL along a direct orbit (red line) or a retrograde orbit (blue line), giving two sets of the relativistic images. Following the approach of [7] enable us to study the observational consequences.

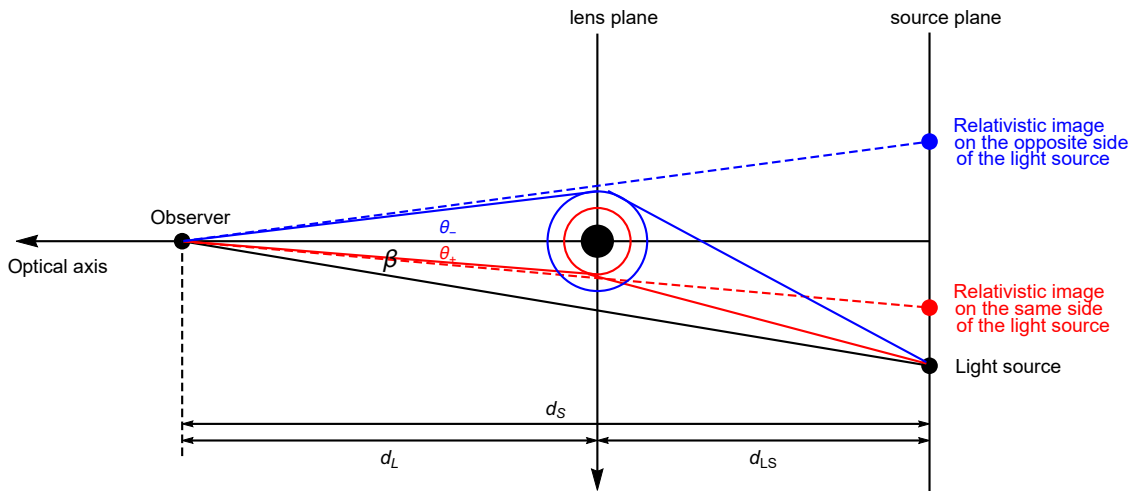


FIG. 1: Gravitational lens about relativistic images. Considering the Kerr or the Kerr Newman black hole with angular momentum of the clockwise rotation, the light rays are emitted from the source, and circle around the black hole multiple times in the SDL along a direct orbit (red line) or a retrograde orbit (blue line). The graph illustrate two sets of the relativistic images.

Layout of the paper is as follows. In Sec.II, we first review the closed-form expression of the deflection angle due to the Kerr and/or the Kerr Newman black holes. In particular, we discuss the results of the radius of the innermost circular motion of light rays as well as the associated critical impact parameters as a function of the black hole's parameters. These will serve as the important inputs to find the values of the coefficients \bar{a} and \bar{b} in the SDL deflection angle. Then we derive the analytic form of \bar{a} and \bar{b} in the cases of Kerr and Kerr-Newman black holes, respectively, and check the consistency with the known results from taking the proper limits of the black holes's parameters. In Sec. III, the analytical

expressions are then applied to compute the angular positions and the magnifications of relativistic images due to the supermassive galactic black holes. The potentially increasing observability of the relativistic images from the effects of angular momentum and charge of the black holes will be summarized in the closing section.

II. DEFLECTION ANGLE DUE TO BLACK HOLES IN THE STRONG DEFLECTION LIMIT

We consider non-spherically symmetric spacetimes of the Kerr and Kerr-Newman metrics respectively to obtain the deflection angle $\hat{\alpha}(b)$ of light rays for a given impact parameter b . In the strong deflection limit (SDL), as $b \rightarrow b_c$, $\hat{\alpha}(b)$ can be approximated in the form as (1) with two parameters \bar{a} and \bar{b} as a function of the black hole's parameters. In what follows, we will consider the above two types of the black holes separately.

A. Kerr black holes

The line element of the Kerr black hole in which spacetime outside a black hole with the gravitational mass M and angular momentum per unit mass $a = J/M$ is described by

$$\begin{aligned} ds^2 &= g_{\mu\nu} dx^\mu dx^\nu \\ &= -\frac{(\Delta - a^2 \sin^2 \theta)}{\Sigma} dt^2 - \frac{a \sin^2 \theta (2Mr)}{\Sigma} (dt d\phi + d\phi dt) \\ &\quad + \frac{\Sigma}{\Delta} dr^2 + \Sigma d\theta^2 + \frac{\sin^2 \theta}{\Sigma} ((r^2 + a^2)^2 - a^2 \Delta \sin^2 \theta) d\phi^2 \end{aligned} \quad (2)$$

with

$$\Sigma = r^2 + a^2 \cos^2 \theta, \quad \Delta = r^2 + a^2 - 2Mr. \quad (3)$$

The outer (inner) event horizon r_+ (r_-) can be found by solving $\Delta(r) = 0$, and is given by

$$r_{\pm} = M \pm \sqrt{M^2 - a^2} \quad (4)$$

with the condition $M^2 > a^2$. Notice that we just adopt the notation of r_- where the light rays traveling outside the horizon are considered.

The Lagrangian of a particle is then

$$\mathcal{L} = \frac{1}{2} g_{\mu\nu} u^\mu u^\nu \quad (5)$$

with the 4-velocity $u^\mu = dx^\mu/d\lambda$ defined in terms of an affine parameter λ . The metric of the Kerr black hole, which is independent on t and ϕ , gives the associated Killing vectors $\xi_{(t)}^\mu$ and $\xi_{(\phi)}^\mu$

$$\xi_{(t)}^\mu = \delta_t^\mu, \quad \xi_{(\phi)}^\mu = \delta_\phi^\mu. \quad (6)$$

Then, together with 4-velocity of light rays, the conserved quantities, namely energy and azimuthal angular momentum, along a geodesic, can be constructed by the above Killing vectors $\varepsilon \equiv -\xi_{(t)}^\mu u_\mu$ and $\ell \equiv \xi_{(\phi)}^\mu u_\mu$, where ε and ℓ are the light ray's energy and azimuthal angular momentum evaluated at spatial infinity. Light rays traveling along null world lines obey the condition $u^\mu u_\mu = 0$. To indicate whether the light rays are traversing along the direction of frame dragging or opposite to it, we define the following impact parameter :

$$b_s = s \left| \frac{\ell}{\varepsilon} \right| \equiv s b, \quad (7)$$

where $s = \text{Sign}(\ell/\varepsilon)$ and b is the positive magnitude. The parameter $s = +1$ for $b_s > 0$ will be referred to as direct orbits, and those with $s = -1$ for $b_s < 0$ as retrograde orbits (see Fig.(1) for the sign convention). Here we restrict the light rays traveling on the equatorial plane of the black hole by choosing $\theta = \pi/2$, and $\dot{\theta} = 0$. The equation of motion along the radial direction can be cast in the form [23]

$$\frac{1}{b^2} = \frac{\dot{r}^2}{\ell^2} + W_{\text{eff}}(r), \quad (8)$$

from which to define the function W_{eff} as

$$W_{\text{eff}}(r) = \frac{1}{r^2} \left[1 - \frac{a^2}{b^2} - \frac{2M}{r} \left(1 - \frac{a}{b_s} \right)^2 \right]. \quad (9)$$

The above equation is analogous to that of particle motion in the effective potential $W_{\text{eff}}(r)$ with the kinetic energy \dot{r}^2/ℓ^2 and constant total energy $1/b^2$. Let us consider that a light ray starts in the asymptotic region to approach the black hole, and then turns back to the asymptotic region to reach the observer. Such light rays have a turning point, the radius of closest approach distance to a black hole r_0 , which crucially depends on the impact parameter b , determined by

$$\left. \frac{\dot{r}^2}{\ell^2} \right|_{r=r_0} = \frac{1}{b^2} - W_{\text{eff}}(r_0) = 0. \quad (10)$$

From (10), also shown in [22, 23], one can find the impact parameter b for a given r_0 , which becomes the important input for the analytical result of the deflection angle in the SDL, as

$$b(r_0) = \frac{2sMa - r_0\sqrt{a^2 - 2r_0M + r_0^2}}{2M - r_0}. \quad (11)$$

The behavior of the light ray trajectories depends on whether $1/b^2$ is greater or less than the maximum height of $W_{\text{eff}}(r)$. The innermost trajectories of light rays have a direct consequence on the apparent shape of the black hole. The smallest radius r_{sc} , when the turning point r_0 is located at the maximum of $W_{\text{eff}}(r)$, for the critical impact parameter b_c , obeys

$$\left. \frac{dW_{\text{eff}}(r)}{dr} \right|_{r=r_{sc}} = 0. \quad (12)$$

Then the radius of a circular motion forming the photon sphere is given by (See [22, 23]).

$$r_{sc} = 2M \left\{ 1 + \cos \left[\frac{2}{3} \cos^{-1} \left(\frac{-sa}{M} \right) \right] \right\} \quad (13)$$

with the corresponding impact parameter

$$b_{sc} = -a + s6M \cos \left[\frac{1}{3} \cos^{-1} \left(\frac{-sa}{M} \right) \right]. \quad (14)$$

In the case of a Kerr black hole, the non-zero spin of the black hole is found to give more repulsive effects to the light rays with the direct orbits than those with the retrograde orbits due to the contribution from the $1/r^3$ term. The repulsive effects in turn affect light rays in the direct orbits in a way to prevent them from collapsing into the event horizon. Thus shifting the innermost circular trajectories of the light rays toward the black hole with the smaller corresponding critical impact parameter b_{+c} than b_{-c} in the retrograde orbits as shown in Fig.(2). As such, when a increases, the impact parameter b_{+c} decreases whereas $|b_{-c}|$ increases instead [22, 23]. It will be shown in the next section that the value of b_{sc} is a key quantity to determine the features of the angular position of the induced images of the distant light sources due to the strong black hole gravitational lensing effects. Also, the presence of black hole's spin is to give the smaller deflection angle in the direct orbits as compared with the retrograde orbits for the same impact parameter b [22, 23].

We proceed by introducing the variable

$$z \equiv 1 - \frac{r_0}{r}. \quad (15)$$

The geodesic equations for r and ϕ found in [23] can be rewritten in terms of z as [12]

$$\frac{dz}{d\phi} = \frac{1}{r_0} \frac{1 - \frac{2M}{r_0}(1-z) + \frac{a^2}{r_0^2}(1-z)^2}{1 - \frac{2M}{r_0}(1-z)(1 - \frac{a}{b_s})} \sqrt{B(z, r_0)}, \quad (16)$$

where the function $B(z, r_0)$ has the trinomial form in z

$$B(z, r_0) = c_1(r_0)z + c_2(r_0)z^2 + c_3(r_0)z^3 \quad (17)$$

with the coefficients

$$\begin{aligned} c_1(r_0) &= -6Mr_0 \left(1 - \frac{a}{b_s}\right)^2 + 2r_0^2 \left(1 - \frac{a^2}{b^2}\right), \\ c_2(r_0) &= 6Mr_0 \left(1 - \frac{a}{b_s}\right)^2 - r_0^2 \left(1 - \frac{a^2}{b^2}\right), \\ c_3(r_0) &= -2Mr_0 \left(1 - \frac{a}{b_s}\right)^2. \end{aligned} \quad (18)$$

Next we rewrite

$$\frac{1 - \frac{2M}{r_0}(1 - \frac{a}{b_s}) + \frac{2M}{r_0}(1 - \frac{a}{b_s})z}{1 - \frac{2M}{r_0} + \frac{a^2}{r_0^2} + (\frac{2M}{r_0} - \frac{2a^2}{r_0^2})z + \frac{a^2}{r_0^2}z^2} = \frac{r_0^2}{a^2} \left(\frac{C_-}{z - z_-} + \frac{C_+}{z - z_+} \right), \quad (19)$$

where the roots z_- , z_+ , and the coefficients C_- , C_+ are

$$\begin{aligned} z_- &= 1 - \frac{r_0 r_-}{a^2}, \\ z_+ &= 1 - \frac{r_0 r_+}{a^2}, \end{aligned} \quad (20)$$

$$\begin{aligned} C_- &= \frac{a^2 - 2Mr_-(1 - \frac{a}{b_s})}{2r_0\sqrt{M^2 - a^2}}, \\ C_+ &= \frac{-a^2 + 2Mr_+(1 - \frac{a}{b_s})}{2r_0\sqrt{M^2 - a^2}} \end{aligned} \quad (21)$$

with r_+ (r_-) being the outer (inner) horizon of a Kerr black hole defined in (4). Also note that z_- , $z_+ \leq 0$, for all spin a . Then the deflection angle can be calculated as a function of the closest approach distance r_0 from (16) giving

$$\hat{\alpha}(r_0) = I(r_0) - \pi, \quad I(r_0) = \int_0^1 f(z, r_0) dz, \quad (22)$$

where the integrand reads as

$$f(z, r_0) = \frac{r_0^2}{a^2} \left(\frac{C_-}{z - z_-} + \frac{C_+}{z - z_+} \right) \frac{2r_0}{\sqrt{c_1(r_0)z + c_2(r_0)z^2 + c_3(r_0)z^3}}. \quad (23)$$

In the SDL of our interest, when the closest approach distance reaches in its critical limit, namely $r_0 \rightarrow r_{sc}$, $c_1(r_0) \rightarrow 0$ in (18) obtained from (12), the integrand $f(z, r_0) \rightarrow \frac{1}{z}$ for small z leads to the logarithmic divergence as $r_0 \rightarrow r_{sc}$. Let us now define a new function $f_D(z, r_0)$

$$f_D(z, r_0) = \frac{r_0^2}{a^2} \left(\frac{C_-}{z - z_-} + \frac{C_+}{z - z_+} \right) \frac{2r_0}{\sqrt{c_1(r_0)z + c_2(r_0)z^2}}, \quad (24)$$

that separates the divergence from the regular part given by $f_R(z, r_0) = f(z, r_0) - f_D(z, r_0)$. The integral of f_D is thus finite.

The divergent part comes from an integral of the function $f_D(z, r_0)$, which contributes not only to \bar{a} for the logarithmic divergence but also \bar{b} for the regular part in (1), giving

$$\begin{aligned} I_D(r_0) &= \int_0^1 f_D(z, r_0) dz \\ &= \frac{2r_0^3}{a^2} \frac{C_-}{\sqrt{c_1(r_0)z_- + c_2(r_0)z_-^2}} \log \left(\frac{\sqrt{c_1(r_0)z_- + c_2(r_0)z_-} + \sqrt{c_1(r_0) + c_2(r_0)z_-}}{\sqrt{c_1(r_0)z_- + c_2(r_0)z_-} - \sqrt{c_1(r_0) + c_2(r_0)z_-}} \right) \\ &\quad + \frac{2r_0^3}{a^2} \frac{C_+}{\sqrt{c_1(r_0)z_+ + c_2(r_0)z_+^2}} \log \left(\frac{\sqrt{c_1(r_0)z_+ + c_2(r_0)z_+} + \sqrt{c_1(r_0) + c_2(r_0)z_+}}{\sqrt{c_1(r_0)z_+ + c_2(r_0)z_+} - \sqrt{c_1(r_0) + c_2(r_0)z_+}} \right). \end{aligned} \quad (25)$$

In the SDL, the expansions of the coefficient $c_1(r_0)$ (18) and the impact parameter $b(r_0)$ in powers of small $r_0 - r_{sc}$ read

$$c_1(r_0) = c'_{1sc}(r_0 - r_{sc}) + O(r_0 - r_{sc})^2, \quad (26)$$

$$b(r_0) = b_{sc} + \frac{b''_{sc}}{2!}(r_0 - r_{sc})^2 + O(r_0 - r_{sc})^3, \quad (27)$$

where $c_1(r_{sc}) \equiv c_{1sc} = 0$ and $b(r_{sc}) \equiv b_{sc}$ is the critical impact parameter b_{sc} given by (14). The subscript sc denotes evaluating the function at $r = r_{sc}$. The prime means the derivative with respect to r_0 . Notice that using $c_{1sc} = 0$ in (18) one finds

$$c_{3sc} = -\frac{2}{3}c_{2sc}. \quad (28)$$

Combining these equations one can write $c_1(r_0)$ in terms of $b - b_{sc}$ as

$$\lim_{r_0 \rightarrow r_{sc}} c_1(r_0) = \lim_{b \rightarrow b_{sc}} c'_{1sc} \sqrt{\frac{2b_{sc}}{b''_{sc}}} \left(\frac{b}{b_{sc}} - 1 \right)^{1/2}. \quad (29)$$

Substituting $c_1(r_0)$ in the SDL into $I_D(r_0)$ (25) becomes

$$I_D(b) \simeq - \left(\frac{r_{sc}^3}{a^2} \frac{C_{-sc}}{\sqrt{c_{2sc} z_{-sc}^2}} + \frac{r_{sc}^3}{a^2} \frac{C_{+sc}}{\sqrt{c_{2sc} z_{+sc}^2}} \right) \log \left(\frac{b}{b_{sc}} - 1 \right) \\ + \frac{r_{sc}^3}{a^2} \frac{C_{-sc}}{\sqrt{c_{2sc} z_{-sc}^2}} \log \left(\frac{16 c_{2sc}^2 z_{-sc}^2 b_{sc}''}{c_{1sc}^2 2b_{sc} (z_{-sc} - 1)^2} \right) + \frac{r_{sc}^3}{a^2} \frac{C_{+sc}}{\sqrt{c_{2sc} z_{+sc}^2}} \log \left(\frac{16 c_{2sc}^2 z_{+sc}^2 b_{sc}''}{c_{1sc}^2 2b_{sc} (z_{+sc} - 1)^2} \right). \quad (30)$$

Finally, the coefficients \bar{a} and the contribution from $I_D(b)$ to \bar{b} denoted by b_D in (1) are

$$\bar{a} = \frac{r_{sc}^3}{\sqrt{c_2}} \left[\frac{C_{-sc}}{r_{sc} r_- - a^2} + \frac{C_{+sc}}{r_{sc} r_+ - a^2} \right] \quad (31)$$

and

$$b_D = \bar{a} \log \left[\frac{8c_{2sc}^2 b_{sc}''}{c_{1sc}^2 b_{sc}} \right] + \frac{2r_{sc}^3}{\sqrt{c_{2sc}}} \left[\frac{C_{-sc}}{r_{sc} r_- - a^2} \log \left(1 - \frac{a^2}{r_{sc} r_-} \right) + \frac{C_{+sc}}{r_{sc} r_+ - a^2} \log \left(1 - \frac{a^2}{r_{sc} r_+} \right) \right], \quad (32)$$

where z_{\pm} are replaced by r_{\pm} through (20). The leading order result in the SDL from the integration of $f_R(z, r_{sc})$ that contributes the coefficient \bar{b} is denoted by b_R with the result

$$b_R = I_R(r_{sc}) = \int_0^1 f_R(z, r_{sc}) dz \\ = \frac{2r_{sc}^3}{a^2} \frac{C_-}{\sqrt{c_2} z_-} \log \left(\frac{z_-}{z_- - 1} \frac{\sqrt{c_2 + c_3} + \sqrt{c_2}}{\sqrt{c_2 + c_3} - \sqrt{c_2}} \frac{c_3}{4c_2} \right) \\ + \frac{2r_{sc}^3}{a^2} \frac{C_-}{\sqrt{c_2 + c_3} z_-} \log \left(\frac{\sqrt{c_2 + c_3} z_- - \sqrt{c_2 + c_3}}{\sqrt{c_2 + c_3} z_- + \sqrt{c_2 + c_3}} \frac{\sqrt{c_2 + c_3} z_- + \sqrt{c_2}}{\sqrt{c_2 + c_3} z_- - \sqrt{c_2}} \right) \\ + \frac{2r_{sc}^3}{a^2} \frac{C_+}{\sqrt{c_2} z_+} \log \left(\frac{z_+}{z_+ - 1} \frac{\sqrt{c_2 + c_3} + \sqrt{c_2}}{\sqrt{c_2 + c_3} - \sqrt{c_2}} \frac{c_3}{4c_2} \right) \\ + \frac{2r_{sc}^3}{a^2} \frac{C_+}{\sqrt{c_2 + c_3} z_+} \log \left(\frac{\sqrt{c_2 + c_3} z_+ - \sqrt{c_2 + c_3}}{\sqrt{c_2 + c_3} z_+ + \sqrt{c_2 + c_3}} \frac{\sqrt{c_2 + c_3} z_+ + \sqrt{c_2}}{\sqrt{c_2 + c_3} z_+ - \sqrt{c_2}} \right) \Big|_{r_0=r_{sc}}. \quad (33)$$

Thus, the coefficient \bar{b} can be calculated as the sum of b_D and b_R

$$\bar{b} = -\pi + b_D + b_R \quad (34)$$

with the help of (32) and (33). In (33) we again use (28) and (20) to replace c_{3sc} by $c_{2sc} = -\frac{2}{3}c_{3sc}$ and z_{\pm} by r_{\pm} . After some straightforward algebra we find

$$\bar{b} = -\pi + \bar{a} \log \left(\frac{36}{7 + 4\sqrt{3}} \frac{8c_{2sc}^2 b_{sc}''}{c_{1sc}^2 b_{sc}} \right) \\ + \frac{r_{sc}^3}{\sqrt{c_{2sc}}} \frac{2aC_{-sc}}{a^2 - r_{sc} r_-} \frac{\sqrt{3}}{\sqrt{a^2 + 2r_{sc} r_-}} \log \left(\frac{\sqrt{a^2 + 2r_{sc} r_-} - a}{\sqrt{a^2 + 2r_{sc} r_-} + a} \frac{\sqrt{a^2 + 2r_{sc} r_-} + \sqrt{3}a}{\sqrt{a^2 + 2r_{sc} r_-} - \sqrt{3}a} \right) \\ + \frac{r_{sc}^3}{\sqrt{c_{2sc}}} \frac{2aC_{+sc}}{a^2 - r_{sc} r_+} \frac{\sqrt{3}}{\sqrt{a^2 + 2r_{sc} r_+}} \log \left(\frac{\sqrt{a^2 + 2r_{sc} r_+} - a}{\sqrt{a^2 + 2r_{sc} r_+} + a} \frac{\sqrt{a^2 + 2r_{sc} r_+} + \sqrt{3}a}{\sqrt{a^2 + 2r_{sc} r_+} - \sqrt{3}a} \right). \quad (35)$$

Using the results of r_{sc} (13), b_{sc} (14) and the expression of $b(r_0)$ (11) together with the definitions of C_{\pm} and c_2 in (21) and (18) respectively, one can compute the coefficients \bar{a} and \bar{b} given by (31) and (35) in (1) of the SDL deflection angle. Notice that within the parameters under investigation $\bar{a} > 0$, but $\bar{b} < 0$. Our results are shown in Fig.(3), where both \bar{a} and $|\bar{b}|$ increase (decrease) in a in the situations of direct (retrograde) orbits, giving the fact that the deflection angle $\hat{\alpha}$ increases (decreases) with the increase of the black hole's spin. Later in section III we will compare with the full numerical computations from (22) in the limit of $b \rightarrow b_{sc}$ when light deflection due the black holes is strong.

The results of \bar{a} and \bar{b} due to the Schwarzschild black hole in [7, 12] can be reproduced by sending $a \rightarrow 0$ where $r_+ \rightarrow 2M$, $r_- \rightarrow a^2/2M$, $C_{+sc} \rightarrow 2M/r_{sc}$, $C_{-sc} \rightarrow a^3/2b_{sc}Mr_{sc}$, and $c_2 \rightarrow r_{sc}^2$ using $c_{1sc} = 0$ in (4) and (21). We can check that $\bar{a} = 1$ in (31) and \bar{b} in (35) reduces to the one proportional to \bar{a} given by

$$\begin{aligned}\bar{b} &= -\pi + \bar{a} \log \left(36(7 - 4\sqrt{3}) \frac{8c_{2sc}^2 b_{sc}''}{c_{1sc}^2 b_{sc}} \right) \\ &= -\pi + \log \left(216(7 - 4\sqrt{3}) \right).\end{aligned}\tag{36}$$

In the second equality above we have used further substitutions $b_{sc} \rightarrow 3\sqrt{3}M$, $b_{sc}'' \rightarrow \sqrt{3}/M$, $c_{1sc}' \rightarrow 6M$, and $c_{2sc} \rightarrow 9M^2$ obtained from $r_{sc} = 3M$ in the Schwarzschild black hole. In Fig.(5), we compare the approximate results of the deflection angle in the SDL with the exact ones in [22] and [23], and find that they are in good agreement when $b \rightarrow b_{sc}$.

The analytical expressions of the coefficient \bar{a} and \bar{b} in the form of the SDL deflection angle due to the Kerr black hole are successfully achieved. They are an extension of the works in [9] and [12] where the spherically symmetric black holes are considered. This is one of the main results in this work.

B. Kerr-Newman black holes

We now consider another example with the non-spherically symmetric metric of a charged spinning black hole. With an addition of charge Q comparing with the Kerr case, the line

element associated with the Kerr-Newman metric is

$$\begin{aligned}
ds^2 &= g_{\mu\nu} dx^\mu dx^\nu \\
&= -\frac{(\Delta - a^2 \sin^2 \theta)}{\Sigma} dt^2 + \frac{a \sin^2 \theta (Q^2 - 2Mr)}{\Sigma} (dt d\phi + d\phi dt) \\
&\quad + \frac{\Sigma}{\Delta} dr^2 + \Sigma d\theta^2 + \frac{\sin^2 \theta}{\Sigma} ((r^2 + a^2)^2 - a^2 \Delta \sin^2 \theta) d\phi^2,
\end{aligned} \tag{37}$$

where

$$\Sigma = r^2 + a^2 \cos^2 \theta, \quad \Delta = r^2 + a^2 + Q^2 - 2Mr. \tag{38}$$

The outer (inner) event horizon r_+ (r_-) is

$$r_{\pm} = M \pm \sqrt{M^2 - (Q^2 + a^2)} \tag{39}$$

with $M^2 > Q^2 + a^2$.

The light rays traveling on the equatorial plane of the black hole have been studied analytically in our previous work in [23], in which the function W_{eff} from the equation of motion along the radial direction in (8) can be regarded as an effective potential given by

$$W_{\text{eff}}(r) = \frac{1}{r^2} \left[1 - \frac{a^2}{b^2} + \left(-\frac{2M}{r} + \frac{Q^2}{r^2} \right) \left(1 - \frac{a}{b_s} \right)^2 \right]. \tag{40}$$

For the Kerr-Newman black hole, the non-zero charge of the black hole is found to give repulsive effects to light rays as seen from its contributions to the function W_{eff} of the $1/r^4$ term, which shifts the innermost circular trajectories of the light rays toward the black holes with the smaller critical impact parameter b_{sc} for both direct and retrograde orbits, as illustrated in Fig.(2). Also, the presence of black hole's charge is to decrease the deflection angle due to the additional repulsive effects on the light rays, as compared with the Kerr case for the same impact parameter b [23]. As we will discuss in the next section, the angular positions of the relativistic images of the distant light sources due to the gravitational lensing of the black holes critically depends on the critical impact parameter b_{sc} .

The impact parameter b as a function of the radius of the circular motion r_0 is obtained as

$$b(r_0) = \frac{s(2aM - a\frac{Q^2}{r_0}) - r_0 \sqrt{(a\frac{Q^2}{r_0^2} - a\frac{2M}{r_0})^2 + (1 - \frac{2M}{r_0} + \frac{Q^2}{r_0^2})[a^2(1 + \frac{2M}{r_0} - \frac{Q^2}{r_0^2}) + r_0^2]}}{2M - r_0 - \frac{Q^2}{r_0}}. \tag{41}$$

The solution of r_{sc} of the radius of the innermost circular motion has been found in [23] as

$$r_{sc} = \frac{3M}{2} + \frac{1}{2\sqrt{3}} \sqrt{9M^2 - 8Q^2 + U_c + \frac{P_c}{U_c}} - \frac{s}{2} \sqrt{6M^2 - \frac{16Q^2}{3} - \frac{1}{3} \left(U_c + \frac{P_c}{U_c} \right) + \frac{8\sqrt{3}Ma^2}{\sqrt{9M^2 - 8Q^2 + U_c + \frac{P_c}{U_c}}}} , \quad (42)$$

where

$$P_c = (9M^2 - 8Q^2)^2 - 24a^2(3M^2 - 2Q^2) ,$$

$$U_c = \left\{ (9M^2 - 8Q^2)^3 - 36a^2(9M^2 - 8Q^2)(3M^2 - 2Q^2) + 216M^2a^4 + 24\sqrt{3}a^2 \sqrt{(M^2 - a^2 - Q^2) [Q^2(9M^2 - 8Q^2)^2 - 27M^4a^2]} \right\}^{\frac{1}{3}} . \quad (43)$$

The analytical expression of the critical value of the impact parameter b_{sc} can be written as a function of black-hole parameters [23],

$$b_{sc} = -a + \frac{M^2a}{2(M^2 - Q^2)} + \frac{s}{2\sqrt{3}(M^2 - Q^2)} \left[\sqrt{V + (M^2 - Q^2) \left(U + \frac{P}{U} \right)} + \sqrt{2V - (M^2 - Q^2) \left(U + \frac{P}{U} \right) - \frac{s6\sqrt{3}M^2a [(M^2 - Q^2)(9M^2 - 8Q^2)^2 - M^4a^2]}{\sqrt{V + (M^2 - Q^2) \left(U + \frac{P}{U} \right)}}} \right] , \quad (44)$$

where

$$P = (3M^2 - 4Q^2) [9(3M^2 - 4Q^2)^3 + 8Q^2(9M^2 - 8Q^2)^2 - 216M^4a^2] ,$$

$$U = \left\{ - [3(3M^2 - 2Q^2)^2 - 4Q^4] [9M^2(9M^2 - 8Q^2)^3 - 8 [3(3M^2 - 2Q^2)^2 - 4Q^4]^2] + 108M^4a^2 [9(3M^2 - 4Q^2)^3 + 4Q^2(9M^2 - 8Q^2)^2 - 54M^4a^2] + 24\sqrt{3}M^2 \sqrt{(M^2 - a^2 - Q^2) [Q^2(9M^2 - 8Q^2)^2 - 27M^4a^2]^3} \right\}^{\frac{1}{3}} ,$$

$$V = 3M^4a^2 + (M^2 - Q^2) [6(3M^2 - 2Q^2)^2 - 8Q^4] . \quad (45)$$

These will serve as the important inputs for the analytical expressions of the coefficients \bar{a} and \bar{b} in the SDL deflection angle as a function of the black hole's parameters.

The counterpart of (16) for the Kerr-Newman case as a function of z in (15) can be easily derived giving

$$\frac{dz}{d\phi} = \frac{1}{r_0} \frac{1 - \frac{2M}{r_0}(1 - z) + \frac{a^2 + Q^2}{r_0^2}(1 - z)^2}{1 - \frac{2M}{r_0}(1 - \frac{a}{b_s})(1 - z) + \frac{Q^2}{r_0^2}(1 - \frac{a}{b_s})(1 - z)^2} \sqrt{B(z, r_0)} , \quad (46)$$

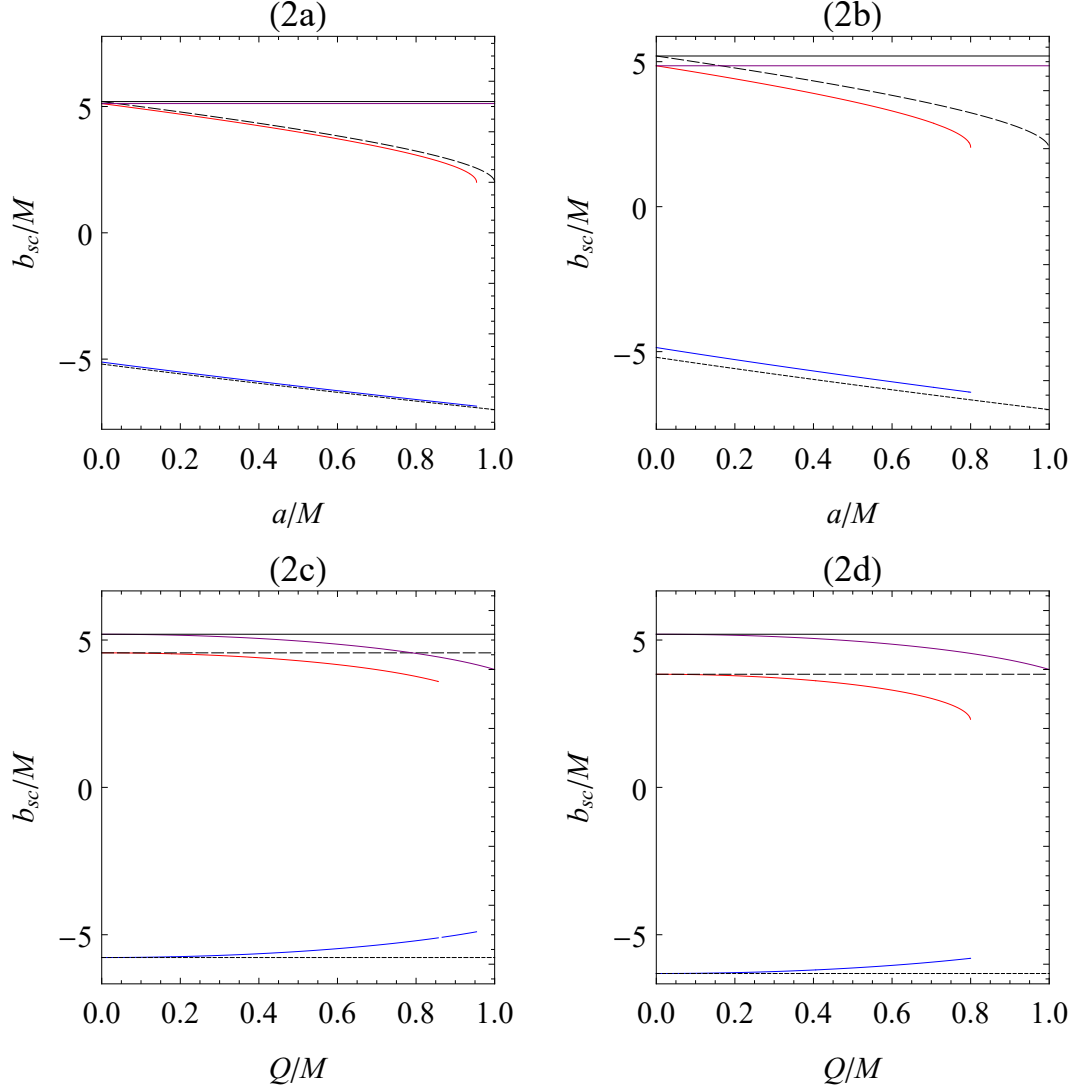


FIG. 2: The critical impact parameter b_{sc}/M as a function of the spin parameter a/M for (a) $Q/M = 0.3$, (b) $Q/M = 0.6$. Also, the critical impact parameter b_{sc}/M as a function of charge Q/M for (c) $a/M = 0.3$, (d) $a/M = 0.6$. The plots show the Schwarzschild, Reissner-Nordström, Kerr and Kerr-Newman black holes for comparison. The plot convention used henceforth: Kerr-Newman direct (solid red line), Kerr-Newman retrograde (solid blue line), Kerr direct (black dashed line with $Q = 0$), Kerr retrograde (black dotted line, with $Q = 0$), Reissner-Nordström (solid purple line, with $a = 0$), and Schwarzschild (solid black line, with $Q = 0, a = 0$).

where

$$B(z, r_0) = c_1(r_0)z + c_2(r_0)z^2 + c_3(r_0)z^3 + c_4(r_0)z^4. \quad (47)$$

The function $B(z, r_0)$ is then the quartic polynomial in z with the coefficients

$$\begin{aligned}
c_1(r_0) &= 4Q^2 \left(1 - \frac{a}{b_s}\right)^2 - 6Mr_0 \left(1 - \frac{a}{b_s}\right)^2 + 2r_0^2 \left(1 - \frac{a^2}{b^2}\right), \\
c_2(r_0) &= -6Q^2 \left(1 - \frac{a}{b_s}\right)^2 + 6Mr_0 \left(1 - \frac{a}{b_s}\right)^2 - r_0^2 \left(1 - \frac{a^2}{b^2}\right), \\
c_3(r_0) &= 4Q^2 \left(1 - \frac{a}{b_s}\right)^2 - 2Mr_0 \left(1 - \frac{a}{b_s}\right)^2, \\
c_4(r_0) &= -Q^2 \left(1 - \frac{a}{b_s}\right)^2.
\end{aligned} \tag{48}$$

All coefficients have the additional contributions from the charge Q . In particular, the presence of the z^4 term with the coefficient $c_4(r_0)$, which vanishes in the Kerr case, makes the calculations of \bar{a} and \bar{b} more involved. The integrant function $f(z, r_0)$ in (22) now takes the form

$$f(z, r_0) = \frac{r_0^2}{a^2 + Q^2} \left(\frac{C_-}{z - z_-} + \frac{C_Q z + C_+}{z - z_+} \right) \frac{2r_0}{\sqrt{c_1(r_0)z + c_2(r_0)z^2 + c_3(r_0)z^3 + c_4(r_0)z^4}}. \tag{49}$$

The corresponding coefficients C_- , C_Q , C_+ in the Kerr-Newman case are

$$\begin{aligned}
C_- &= \frac{a^2 + Q^2 - 2Mr_-(1 - \frac{a}{b_s}) + \frac{Q^2 r_-^2}{a^2 + Q^2} (1 - \frac{a}{b_s})}{2r_0 \sqrt{M^2 - a^2 - Q^2}}, \\
C_Q &= \frac{Q^2}{r_0^2} \left(1 - \frac{a}{b_s}\right), \\
C_+ &= \frac{a^2 + Q^2 - 2Mr_-(1 - \frac{a}{b_s}) + \frac{Q^2}{r_0} (r_+ - r_-) (1 - \frac{a}{b_s}) + Q^2 (1 - \frac{a}{b_s})}{-2r_0 \sqrt{M^2 - a^2 - Q^2}},
\end{aligned} \tag{50}$$

where z_+ , z_- then become

$$\begin{aligned}
z_- &= 1 - \frac{r_0 r_-}{a^2 + Q^2}, \\
z_+ &= 1 - \frac{r_0 r_+}{a^2 + Q^2},
\end{aligned} \tag{51}$$

defined in terms of the outer(inner) black hole horizon r_+ (r_-). Again, $z_{\pm} \leq 0$ for all a and Q with the nonzero r_+ . Note that, for charge $Q \rightarrow 0$, C_Q vanishes.

Analog to the previous subsection of the Kerr case, we define the function $f_D(z, r_0)$ as

$$f_D(z, r_0) = \frac{r_0^2}{a^2 + Q^2} \left(\frac{C_-}{z - z_-} + \frac{C_Q z + C_+}{z - z_+} \right) \frac{2r_0}{\sqrt{c_1(r_0)z + c_2(r_0)z^2}}. \tag{52}$$

As $z \rightarrow 0$, $f_D(z, r_0) \rightarrow 1/z$, its integration over z gives the divergent part of $I_D(r_0)$ when $b \rightarrow b_c$. For the integral we find

$$\begin{aligned}
I_D(r_0) &= \int_0^1 f_D(z, r_0) dz \\
&= \frac{2r_0^3}{a^2 + Q^2} \frac{C_-}{\sqrt{c_1(r_0)z_- + c_2(r_0)z_-^2}} \log \left(\frac{\sqrt{c_1(r_0)z_- + c_2(r_0)z_-} + \sqrt{c_1(r_0) + c_2(r_0)z_-}}{\sqrt{c_1(r_0)z_- + c_2(r_0)z_-} - \sqrt{c_1(r_0) + c_2(r_0)z_-}} \right) \\
&\quad + \frac{2r_0^3}{a^2 + Q^2} \frac{C_+ + C_Q z_+}{\sqrt{c_1(r_0)z_+ + c_2(r_0)z_+^2}} \log \left(\frac{\sqrt{c_1(r_0)z_+ + c_2(r_0)z_+} + \sqrt{c_1(r_0) + c_2(r_0)z_+}}{\sqrt{c_1(r_0)z_+ + c_2(r_0)z_+} - \sqrt{c_1(r_0) + c_2(r_0)z_+}} \right) \\
&\quad - \frac{2r_0^3}{a^2 + Q^2} \frac{2C_Q}{\sqrt{c_2(r_0)}} \log \left(\sqrt{c_1(r_0)} \sqrt{c_2(r_0)} \right) \\
&\quad + \frac{2r_0^3}{a^2 + Q^2} \frac{2C_Q}{\sqrt{c_2(r_0)}} \log \left(c_2(r_0) + \sqrt{c_2(r_0)} \sqrt{c_1(r_0) + c_2(r_0)} \right).
\end{aligned} \tag{53}$$

In the SDL by substituting the expansion in (26) and (29), $I_D(b)$ becomes

$$\begin{aligned}
I_D(b) &\approx - \frac{r_{sc}^3}{a^2 + Q^2} \left(\frac{C_{-sc}}{\sqrt{c_{2sc}z_{-sc}^2}} + \frac{C_{+sc} + C_{Qsc}z_{+sc}}{\sqrt{c_{2sc}z_{+sc}^2}} + \frac{C_{Qsc}}{\sqrt{c_{2sc}}} \right) \log \left(\frac{b}{b_{sc}} - 1 \right) \\
&\quad + \frac{r_{sc}^3}{a^2 + Q^2} \frac{C_{-sc}}{\sqrt{c_{2sc}z_{-sc}^2}} \log \left[\frac{16c_{2sc}^2 z_{-sc}^2 b_{sc}''}{c_{1sc}^2 2b_{sc}(z_{-sc} - 1)^2} \right] \\
&\quad + \frac{r_{sc}^3}{a^2 + Q^2} \frac{C_{+sc} + C_{Qsc}z_{+sc}}{\sqrt{c_{2sc}z_{+sc}^2}} \log \left[\frac{16c_{2sc}^2 z_{+sc}^2 b_{sc}''}{c_{1sc}^2 2b_{sc}(z_{+sc} - 1)^2} \right] + \frac{r_{sc}^3}{a^2 + Q^2} \frac{C_{Qsc}}{\sqrt{c_{2sc}}} \log \left[\frac{16c_{2sc}^2 b_{sc}''}{c_{1sc}^2 2b_{sc}} \right],
\end{aligned} \tag{54}$$

from which we can read off the coefficients \bar{a} and b_D as follows

$$\bar{a} = \frac{r_{sc}^3}{\sqrt{c_{2sc}}} \left[\frac{C_{-sc}}{r_{sc}r_- - (a^2 + Q^2)} + \frac{C_{+sc}}{r_{sc}r_+ - (a^2 + Q^2)} \right] \tag{55}$$

$$\begin{aligned}
b_D &= \bar{a} \log \left[\frac{8c_{2sc}^2 b_{sc}''}{c_{1sc}^2 b_{sc}} \right] \\
&\quad + \frac{2r_{sc}^3}{\sqrt{c_{2sc}}} \left[\frac{C_{-sc}}{r_{sc}r_- - (a^2 + Q^2)} \log \left(1 - \frac{a^2 + Q^2}{r_{sc}r_-} \right) + \frac{C_{+sc} + C_{Qsc}z_{+sc}}{r_{sc}r_+ - (a^2 + Q^2)} \log \left(1 - \frac{a^2 + Q^2}{r_{sc}r_+} \right) \right].
\end{aligned} \tag{56}$$

They reduce to their counterparts in (31) and (32) respectively as $Q \rightarrow 0$, and thus $C_Q \rightarrow 0$.

As for the remaining contributions to the regular part, and in the SDL, we find that

$$\begin{aligned}
b_R &= I_R(r_{sc}) = \int_0^1 f_R(z, r_{sc}) dz \\
&= \frac{2r_{sc}^3}{a^2 + Q^2} \frac{C_-}{\sqrt{c_2} z_-} \log \left(\frac{z_-}{z_- - 1} \frac{2c_2 + c_3 + 2\sqrt{c_2 + c_3 + c_4}\sqrt{c_2}}{4c_2} \right) \\
&+ \frac{2r_{sc}^3}{a^2 + Q^2} \frac{C_-}{z_- \sqrt{c_2 + c_3 z_- + c_4 z_-^2}} \log \left(\frac{z_- - 1}{z_-} \frac{\left(\sqrt{c_2 + c_3 z_- + c_4 z_-^2} + \sqrt{c_2} \right)^2 - c_4 z_-^2}{\left(\sqrt{c_2 + c_3 z_- + c_4 z_-^2} + \sqrt{c_2 + c_3 + c_4} \right)^2 - c_4 (z_- - 1)^2} \right) \\
&+ \frac{2r_{sc}^3}{a^2 + Q^2} \frac{C_+}{\sqrt{c_2} z_+} \log \left(\frac{z_+}{z_+ - 1} \frac{2c_2 + c_3 + 2\sqrt{c_2 + c_3 + c_4}\sqrt{c_2}}{4c_2} \right) \\
&+ \frac{2r_{sc}^3}{a^2 + Q^2} \frac{C_+ + C_Q z_+}{z_+ \sqrt{c_2 + c_3 z_+ + c_4 z_+^2}} \log \left(\frac{z_+ - 1}{z_+} \frac{\left(\sqrt{c_2 + c_3 z_+ + c_4 z_+^2} + \sqrt{c_2} \right)^2 - c_4 z_+^2}{\left(\sqrt{c_2 + c_3 z_+ + c_4 z_+^2} + \sqrt{c_2 + c_3 + c_4} \right)^2 - c_4 (z_+ - 1)^2} \right) \\
&+ \frac{2r_{sc}^3}{a^2 + Q^2} \frac{C_Q}{\sqrt{c_2}} \log \left(\frac{z_+}{z_+ - 1} \right) \Big|_{r_0=r_{sc}}
\end{aligned} \tag{57}$$

In the limit of $Q \rightarrow 0$, where C_Q and c_4 go to zero, the above expression of b_R reduces to (33) in the Kerr case after implementing straightforward algebra. The coefficient \bar{b} is obtained using (56) and (57) as

$$\begin{aligned}
\bar{b} &= -\pi + \bar{a} \log \left[\frac{36}{4(1 - c_{4sc}/c_{2sc})^2 + 4\sqrt{3}(1 - c_{4sc}/c_{2sc})^{3/2} + 3(1 - c_{4sc}/c_{2sc})} \frac{8c_{2sc}^2 b_{sc}''}{c_{1sc}^2 b_{sc}} \right] \\
&+ \frac{r_{sc}^3}{\sqrt{c_{2sc}}} \frac{2(a^2 + Q^2)C_{-sc}}{(a^2 + Q^2 - r_{sc}r_-)} \frac{\sqrt{3}}{P_-} \\
&\times \log \left[\frac{-r_{sc}r_-}{a^2 + Q^2 - r_{sc}r_-} \frac{(P_- + \sqrt{3}(a^2 + Q^2))^2 - 3(a^2 + Q^2 - r_{sc}r_-)^2 (c_{4sc}/c_{2sc})}{(P_- + (a^2 + Q^2)(1 - c_{4sc}/c_{2sc})^{1/2})^2 - 3r_{sc}^2 r_-^2 (c_{4sc}/c_{2sc})} \right] \\
&+ \frac{r_{sc}^3}{\sqrt{c_{2sc}}} \frac{2[(a^2 + Q^2)C_{+sc} + (a^2 + Q^2 - r_{sc}r_+)C_{Qsc}]}{(a^2 + Q^2 - r_{sc}r_+)} \frac{\sqrt{3}}{P_+} \\
&\times \log \left[\frac{-r_{sc}r_+}{a^2 + Q^2 - r_{sc}r_+} \frac{(P_+ + \sqrt{3}(a^2 + Q^2))^2 - 3(a^2 + Q^2 - r_{sc}r_+)^2 (c_{4sc}/c_{2sc})}{(P_+ + (a^2 + Q^2)(1 - c_{4sc}/c_{2sc})^{1/2})^2 - 3r_{sc}^2 r_+^2 (c_{4sc}/c_{2sc})} \right]
\end{aligned} \tag{58}$$

In the equation above, we have replaced c_{3sc} by the linear combination of c_{2sc} and c_{4sc} in (48),

$$c_{3sc} = -\frac{2}{3}c_{2sc} - \frac{4}{3}c_{4sc}. \tag{59}$$

We also have

$$P_{\pm}^2 = (a^2 + Q^2 + 2r_{sc}r_{\pm})(a^2 + Q^2) - (a^2 + Q^2 + r_{sc}r_{\pm})(a^2 + Q^2 - r_{sc}r_{\pm})(c_{4sc}/c_{2sc}). \quad (60)$$

Combining (41), (42) and (44), the coefficients \bar{a} and \bar{b} in (55) and (58) can be analytically expressed as a function of the black hole's parameters in the SDL. Our results are shown in Fig.(4). Again, notice that $\bar{a} > 0$ but $\bar{b} < 0$ with the parameters in the figure. Due to the fact that the bending angle for light rays given by the charged black hole is suppressed as compared with the corresponding black hole with $Q = 0$ for the same impact parameter b , both \bar{a} and $|\bar{b}|$ are found to increase with the charge Q .

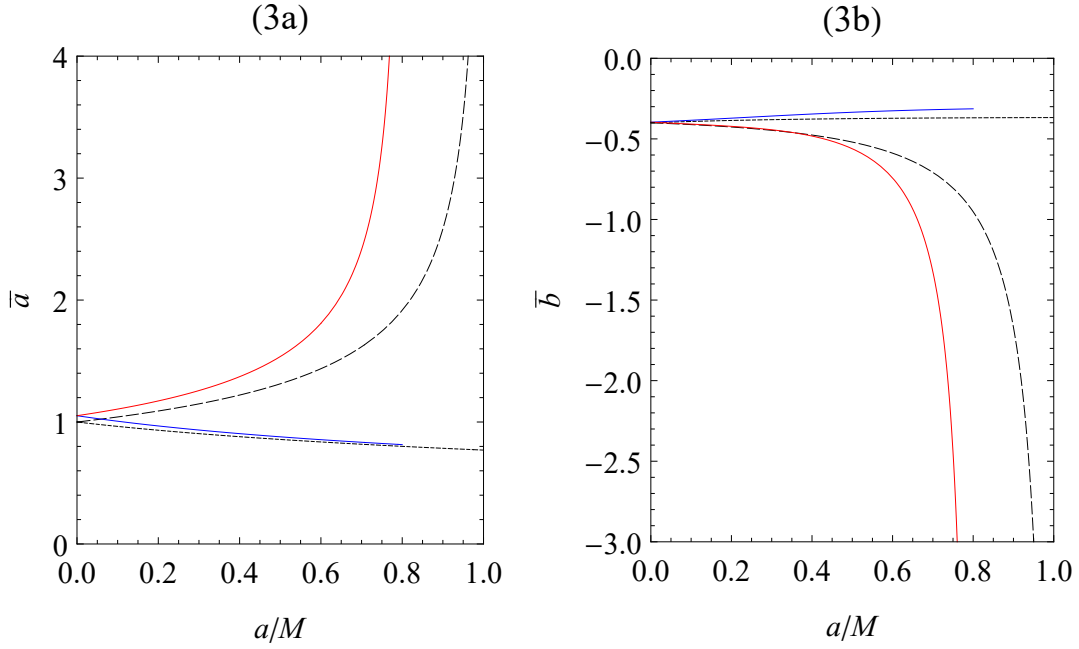


FIG. 3: The coefficients \bar{a} and \bar{b} as a function of the spin parameter a/M for the Kerr black hole with $Q/M = 0$ and the Kerr Newman black hole with $Q/M = 0.6$.

It is then quite straightforward to check that the coefficients \bar{a} and \bar{b} in the Kerr-Newmann case can reduce to those in (31) and (35) in the Kerr case by setting $c_4 \rightarrow 0$ in the limit of $Q \rightarrow 0$, also leading to $P_{\pm} \rightarrow a\sqrt{a^2 + 2r_{sc}r_{\pm}}$. To compare with the Reissner-Nordström black hole of works [12, 13], it is known that the impact parameter b as a function of r_0 is

$$b(r_0) = \frac{r_0^2}{\sqrt{Q^2 - 2Mr_0 + r_0^2}} \quad (61)$$

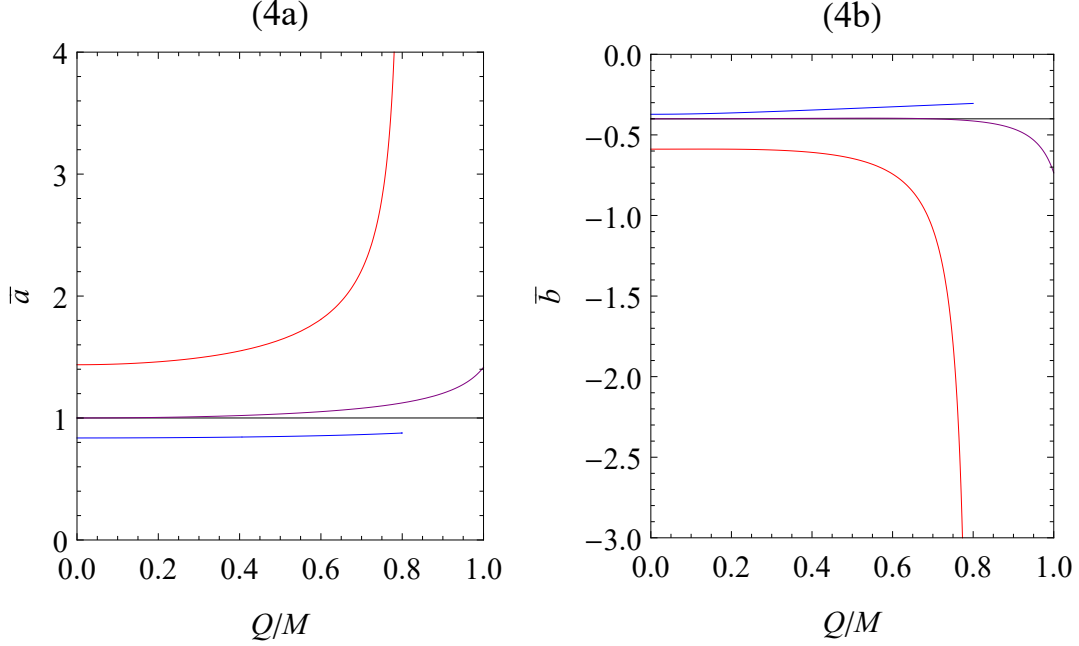


FIG. 4: The coefficients of \bar{a} and \bar{b} as a function of charge Q/M for the the Reissner-Nordström black hole with $a/M = 0$ and the Kerr-Newman black hole with $a/M = 0.6$.

and the circular motion of light rays forms the photon sphere with the radius

$$r_c = \frac{3M + \sqrt{9M^2 - 8Q^2}}{2} . \quad (62)$$

The critical impact parameter as a function of r_c read as

$$b_c = \frac{r_c^2}{\sqrt{Mr_c - Q^2}} . \quad (63)$$

Notice the subscript is changed from sc to c since the same critical impact parameters are obtained for light rays with direct orbits and retrograde orbits in the case of the non-spinning black holes. In the limit of $a \rightarrow 0$, we have $C_{-sc} \rightarrow 0$ in (50) using the definition of r_- in (39). Thus, the coefficient \bar{a} in (55) can be further simplified using (50), (39) and $c_{1sc} = 0$ giving

$$\bar{a} = \frac{r_c}{\sqrt{3Mr_c - 4Q^2}} , \quad (64)$$

which reproduces the same expression as in [12, 13]. As for the coefficient \bar{b} , in the limit of $a \rightarrow 0$, apart from $C_{-sc} \rightarrow 0$, $(a^2 + Q^2)C_{+sc} + (a^2 + Q^2 - r_{sc}r_+)C_{Qsc} \rightarrow 0$ as well. So, the coefficient \bar{b} in (58) has the contribution only from the term proportional to \bar{a} . After

substituting (61) and (48) in the limit of $a \rightarrow 0$ to (58) and going through nontrivial algebra, we indeed recover the compact analytical expression obtained in [12, 13]:

$$\bar{b} = -\pi + \bar{a} \log \left[\frac{8(3Mr_c - 4Q^2)^3}{M^2 r_c^2 (Mr_c - Q^2)^2} \left(2\sqrt{Mr_c - Q^2} - \sqrt{3Mr_c - 4Q^2} \right)^2 \right]. \quad (65)$$

Fig.(5) shows good agreement between the obtained SDL expression and the exact one in [23] computed numerically when b approaches b_c for some values of a and Q .

In conclusion, we have successfully obtained the analytical expression of the coefficient \bar{a} and \bar{b} in the form (1) of the SDL deflection angle due to the spherically non-symmetric black holes with finite angular momentum a and charge Q , although they look not as simple as the cases due to the spherically symmetric black holes. Additionally, the obtained expressions can reproduce the respective ones due to the Kerr, Reissner-Nordström black holes and further due to the Schwarzschild black hole by taking the appropriate limits of the black hole's parameters.

III. RELATIVISTIC IMAGES OF GRAVITATIONAL LENS AND APPLICATIONS TO SUPERMASSIVE GALACTIC BLACK HOLES

We consider the cases of the planar light rays with the lens diagram shown in Fig.(1), where d_L and d_S are the distances of the lens (black hole) and the light source from the observer, and also d_{LS} represents the distance between the lens and the source. The line joining the observer and the lens is considered as a reference optical axis. The angular positions of the source and the image are measured from the optical axis, and are denoted by β and θ , respectively. The lens equation is given by [4]

$$\tan s\beta = \tan \theta - \frac{d_{LS}}{d_S} [\tan \theta + \tan(\hat{\alpha} - \theta)], \quad (66)$$

where $\hat{\alpha}$ is the deflection angle of light rays obtained from (22) that can be expressed in terms of the impact parameter b as the light rays approach to the black holes. In the SDL of our interest when the light rays wind around the black hole n times, the deflection angle $\hat{\alpha}$ can be approximately by (1). The angle appearing in the lens equation should be within 2π and can be obtained from the deflection angle $\hat{\alpha}$ subtracting $2n\pi$.

Together with the relation between the impact parameter b and the angular position of the image given by

$$b = d_L \sin \theta, \quad (67)$$

based upon the lens diagram in Fig.(1), we can solve the lens equation (66) with a given angular position of the source β for the angular position of the observed image θ . In the SDL, when the angular position of the source is small, θ is expectedly small with the small impact parameter b . Then the lens equation (66) can be further simplified by

$$s\beta \simeq \theta - \frac{d_{LS}}{d_S} [\hat{\alpha}(\theta) - 2n\pi] \quad (68)$$

with (67) replaced using the approximation $b \simeq d_L \theta$. According to [9], the zeroth order solution θ_{sn}^0 is obtained from $\hat{\alpha}(\theta_{sn}^0) = 2n\pi$. Using the SDL deflection angle in (1) we have then

$$\theta_{sn}^0 = \frac{|b_{sc}|}{d_L} \left(1 + e^{\frac{\bar{b}-2n\pi}{\bar{a}}} \right) \quad (69)$$

for $n = 1, 2, \dots$. The angular position θ_{sn} decrease in n and reaches the asymptotic angular position given by $\theta_{s\infty} = |b_{sc}|/d_L$ as $n \rightarrow \infty$. With the zeroth order solution (69), the expansion of $\hat{\alpha}(\theta)$ around $\theta = \theta_{sn}^0$ is written explicitly as

$$\hat{\alpha}(\theta) = \hat{\alpha}(\theta_{sn}^0) - \frac{\bar{a}}{e^{(\bar{b}-2n\pi)/\bar{a}}} \frac{d_L d_{LS}}{|b_{sc}| d_S} (\theta - \theta_{sn}^0) + O(\theta - \theta_{sn}^0)^2. \quad (70)$$

Then the approximate lens equation (68) to the order $(\theta - \theta_{sn}^0)$ becomes

$$s\beta \simeq \theta_{sn}^0 + \left(1 + \frac{\bar{a}}{e^{(\bar{b}-2n\pi)/\bar{a}}} \frac{d_L d_{LS}}{|b_{sc}| d_S} \right) (\theta - \theta_{sn}^0). \quad (71)$$

Solving for θ , by keeping the lowest order term in $|b_{sc}|/d_L \ll 1$, we find the angular position of the image as [7]

$$\theta_{sn} \simeq \theta_{sn}^0 + \frac{e^{(\bar{b}-2n\pi)/\bar{a}}}{\bar{a}} \frac{|b_{sc}| d_S}{d_{LS} d_L} (s\beta - \theta_{sn}^0). \quad (72)$$

We assume that either Kerr or Kerr-Newman black holes have the clockwise rotation in Fig.(1). The light rays emitted from the source circle around the black hole multiple times in the SDL along a direct orbit (red line) with $s = +1$, where both the image and the source end up on the same sides of the optical axis with the angular position θ_{+n} and/or along a retrograde orbit (blue line) with $s = -1$, where the image and the source are on the opposite sides with the angular position θ_{-n} . We define next the angular position difference between the outermost image $\theta_{1\pm}$ and the asymptotic one near the optical axis as

$$\Delta\theta_s = \theta_{s1} - \theta_{s\infty}, \quad (73)$$

which are the values to compare with the resolution of the observation for being able to distinguish among a set of the relativistic images in either sides of the optical axis. Light rays are deflected due to gravitation fields, which cause the change of the cross section of a bundle of rays. The magnifications of the images μ defined to be the ratio of the flux of the image to the flux of the source can then be obtained from the ratio of the solid angles of the images and the sources, and are given and further approximated in the SDL as

$$\mu = \left(\frac{\sin \beta}{\sin \theta} \frac{d\beta}{d\theta} \right)^{-1} \approx \left(\frac{\beta}{\theta} \frac{d\beta}{d\theta} \right)^{-1}. \quad (74)$$

For the image with the angular position θ_{sn} , the magnification μ_{sn} is found to be [7]

$$\mu_{sn} \simeq \frac{e^{(\bar{b}-2n\pi)/\bar{a}}}{\bar{a}} \frac{|b_{sc}| d_S}{d_L d_{LS}} \frac{\theta_{sn}^0}{\beta}. \quad (75)$$

Apart from very small β , where the source and the lens are extremely aligned, μ normally is very small due to $|b_{sc}| \ll d_L$. It implies the demagnification of the images and thus causes difficulties in observing the relativistic images.

In this work we compute the angular positions and the magnifications of the relativistic images of the sources for $n = 1$ (the outermost image) due to either Kerr or Kerr-Newman black holes with the mass $M = 4.1 \times 10^6 M_\odot$ and the distance $d_L = 26000$ ly of the super-massive black hole Sagittarius A* at the center of our galaxy as an example. We also take the ratio to be $d_{LS}/d_S = 1/2$. In Table 1 (2), we consider both the image and the source are in the same (opposite) sides of the optical axis, where the light rays travel along the direct (retrograde) orbits, and choose $\beta \sim \theta_{\pm 1}$. The angular positions of the relativistic images are computed by (72). In the case of $|b_{sc}| \ll d_L$, θ_{sn} is not sensitive to β but mainly determined by θ_{sn}^0 in (69). For \bar{a} and $|\bar{b}|$ of order given in Figs.(3) and (4), $e^{-\frac{|\bar{b}|+2n\pi}{\bar{a}}} \ll 1$ for $\bar{a} > 0$ and $\bar{b} < 0$. The behavior of θ_{sn} thus depends mainly on $|b_{sc}|$ as a function of angular momentum a and charge Q of the black holes.

As discussed in the previous section, since the contribution from the angular momentum for direct orbits effectively induces more repulsive effects compared with the retrograde orbits, clearly shown in their effective potential W_{eff} (9), the resulting $b_{+c} < |b_{-c}|$ yields asymmetric values of $\theta_{+1} < \theta_{-1}$ for the same a and Q . These features are shown in the Tables 1 and 2. Additionally, we notice that θ_{+1} (θ_{-1}) decreases (increases) in a for fixed Q resulting from the decrease (increase) of b_{+c} ($|b_{-c}|$) as a increases. As for $\Delta\theta$, $\Delta\theta_+ > \Delta\theta_-$ for the same a and Q . Moreover, for the same Q , $\Delta\theta_+$ increases with a whereas $\Delta\theta_-$ decreases with

a/M	Q/M	θ_{+1} (μas)	$\hat{\alpha}$	b/M	μ_{+1}	$\theta_{+\infty}$ (μas)	$\Delta\theta_+$ (μas)
10^{-3}	10^{-3}	26.4231	$2\pi + 32.8135$ (μas)	5.2007	8.47943×10^{-13}	26.3900	0.0331
	0.3	26.0217	$2\pi + 32.0563$ (μas)	5.1217	8.74379×10^{-13}	25.9866	0.0351
	0.6	24.7179	$2\pi + 29.4336$ (μas)	4.8651	9.83900×10^{-13}	24.6747	0.0432
	0.8	23.1445	$2\pi + 26.2837$ (μas)	4.5554	1.19045×10^{-12}	23.0849	0.0596
0.5	10^{-3}	20.9290	$2\pi + 21.8561$ (μas)	4.1193	1.80864×10^{-12}	20.8119	0.1171
	0.3	20.4085	$2\pi + 20.8203$ (μas)	4.0169	1.94376×10^{-12}	20.2758	0.1327
	0.6	18.6189	$2\pi + 17.2398$ (μas)	3.6646	2.51420×10^{-12}	18.4049	0.2140
	0.8	16.0922	$2\pi + 12.1835$ (μas)	3.1673	3.89740×10^{-12}	15.5372	0.5550
0.9	10^{-3}	15.1170	$2\pi + 10.2354$ (μas)	2.9754	3.77464×10^{-12}	14.4517	0.6653
	0.3	14.1818	$2\pi + 8.36638$ (μas)	2.7913	3.74794×10^{-12}	13.2701	0.9117
	0.6	-	-	-	-	-	-
	0.8	-	-	-	-	-	-

TABLE I: Relativistic images on the same side of the source with the angular position $\beta = 10$ (μas) where the light rays are with direct orbits seen in Fig.(1).

a . In particular, $\Delta\theta_+$ can increase from about $10^{-2}\mu\text{as}$ with $a/M \sim 10^{-3}$ and $Q/M = 10^{-3}$ to the value as high as $0.6\mu\text{as}$ with $a/M = 0.9$ and $Q/M = 10^{-3}$, which certainly increases their observability by the current very long baseline interferometry (VLBI) [29, 30]. As for the finite Q , also showing the repulsive effects seen in the effective potential (40), both θ_{+1} and θ_{-1} decrease in Q for fixed a , resulting in the slightly increase in $\Delta\theta_{\pm}$.

The magnifications of the relativistic images at the angular position θ_{sn} can be calculated from (75), and their dependence of the black hole's parameters is determined by the coefficients \bar{a} and \bar{b} , mainly through $\mu \propto e^{-2n\pi/\bar{a}}$ since typically $|\bar{b}| < 2\pi$. In the case of $n = 1$, the increase (decrease) of \bar{a} for direct (retrograde) orbits as a increases by fixing Q drives the increase (decrease) in the magnification μ_{+1} (μ_{-1}), as shown in Tables 1 and 2 respectively. In particular, μ_{+1} for direct orbits can be increased from 10^{-13} with $a/M = 10^{-3}$ and $Q/M = 10^{-3}$ to 10^{-12} with $a/M = 0.9$ and $Q/M = 10^{-3}$. Similar discussions are also applied to the charge Q of the black hole with fixed angular momentum a . The increase of \bar{a} as Q increases for both direct and retrograde orbits results in the increase of μ_{\pm} also shown in the Tables. For example, $\mu_{\pm 1}$ can also be increased from 10^{-13} with $a/M = 10^{-3}$

a/M	Q/M	θ_{-1} (μas)	$\hat{\alpha}$	b/M	μ_{-1}	$\theta_{-\infty}$ (μas)	$\Delta\theta_{-}$ (μas)
10^{-3}	10^{-3}	26.4433	$2\pi + 72.8286$ (μas)	5.20464	8.45698×10^{-13}	26.4103	0.0330
	0.3	26.0422	$2\pi + 72.0654$ (μas)	5.12569	8.71996×10^{-13}	26.0073	0.0349
	0.6	24.7395	$2\pi + 69.4844$ (μas)	4.86931	9.80915×10^{-13}	24.6966	0.0429
	0.8	23.1680	$2\pi + 66.3165$ (μas)	4.56000	1.18618×10^{-12}	23.1088	0.0592
0.5	10^{-3}	31.1994	$2\pi + 82.4458$ (μas)	6.14075	4.65797×10^{-13}	31.1862	0.0132
	0.3	30.8561	$2\pi + 81.6482$ (μas)	6.07318	4.81067×10^{-13}	30.8422	0.0139
	0.6	29.7638	$2\pi + 79.5352$ (μas)	5.85820	5.23292×10^{-13}	29.7479	0.0159
	0.8	28.5058	$2\pi + 76.9916$ (μas)	5.61059	5.87384×10^{-13}	28.4866	0.0192
0.9	10^{-3}	34.7203	$2\pi + 89.4397$ (μas)	6.83374	3.09898×10^{-13}	34.7130	0.0073
	0.3	34.4063	$2\pi + 88.5984$ (μas)	6.77195	3.19041×10^{-13}	34.3988	0.0075
	0.6	-	-	-	-	-	-
	0.8	-	-	-	-	-	-

TABLE II: Relativistic images on the opposite side of the source with the angular position $\beta = 10$ (μas) where the light rays are with retrograde orbits seen in Fig.(1).

and $Q/M = 10^{-3}$ to 10^{-12} with $a/M = 10^{-3}$ and $Q/M = 0.8$. The effects from angular momentum a and charge Q of the black holes with the enhanced μ values may increase the visibility of the created images.

IV. SUMMARY AND OUTLOOK

In summary, the dynamics of light rays traveling around the Kerr black hole and the Kerr-Newman black hole, respectively, is studied with the detailed derivations on achieving analytical expressions of \bar{a} and \bar{b} in the approximate form of the deflection angle in the SDL. Various known results are checked by taking the proper limits of the black hole's parameters. The analytical expressions are then applied to compute the angular positions and the magnifications of relativistic images due to the supermassive galactic black holes. We find that the effects from the angular momentum a for direct orbits of light rays and the charge Q for both direct and retrograde orbits increase the angular separation of the outermost images from the others and the magnification. Although the observation of relativistic images is a

very difficult task [29], our studies show potentially increasing observability of the relativistic images from the effects of angular momentum and charge of the black holes. Hopefully, relativistic images will be observed in the near future. Through the analytical results we present in this work, one can reconstruct the black hole's parameters that give strong lensing effects. Inspired by the recent advent of horizon-scale observations of astrophysical black holes, the properties of null geodesics become of great relevance to astronomy. The recent work of [30–32] provides an extensive analysis on Kerr black holes. In the next step, we will extend the analysis of null geodesic to Kerr-Newman black holes, focusing on the effects from the charge of black holes.

Acknowledgments

This work was supported in part by the Ministry of Science and Technology, Taiwan, under Grant No.108-2112-M-259-002 and 109-2813-C-259-008-M.

-
- [1] C. W. Misner, K. S. Thorne, and J. A. Wheeler, *Gravitation* (W. H. Freeman and Company, San Francisco, 1973).
 - [2] J. B. Hartle, *Gravity: An Introduction to Einstein's General Relativity* (Addison-Wesley, 2003).
 - [3] P. Schneider, J. Ehlers, and E. E. Falco, *Gravitational Lenses* (Springer-Verlag, New York, Berlin, Heidelberg, 1992).
 - [4] K. S. Virbhadra and G. F. R. Ellis, Schwarzschild black hole lensing, *Phys. Rev. D* 62, 084003 (2000).
 - [5] Simonetta Frittelli, Thomas P. Kling, and Ezra T. Newman, Spacetime perspective of Schwarzschild lensing, *Phys. Rev. D* 61, 064021 (2000).
 - [6] V. Bozza, S. Capozziello, G. Iovane, and G. Scarptta, Strong field limit of black hole gravitational lensing, *Gen. Relativ. Gravit.* 33, 1535 (2001).
 - [7] V. Bozza, Gravitational lensing in the strong field limit, *Phys. Rev. D* 66, 103001 (2002).
 - [8] V. Bozza, Quasiequatorial gravitational lensing by spinning black holes in the strong field limit, *Phys. Rev. D* 67, 103006 (2003).
 - [9] V. Bozza, Gravitational lensing by black holes, *Gen. Relativ. Gravit.* 42, 2269 (2010).

- [10] Ernesto F. Eiroa, Gustavo E. Romero, and Diego F. Torres, Reissner-Nordström black hole lensing, *Phys. Rev. D* 66, 024010 (2002).
- [11] S. V. Iyer and A. O. Petters, Light's Bending Angle due to Black Holes: From the Photon Sphere to Infinity, *Gen. Relativ. Gravit.* 39, 1563 (2007).
- [12] N. Tsukamoto, Deflection angle in the strong deflection limit in a general asymptotically flat, static, spherically symmetric space-time, *Phys. Rev. D* 95, 064035 (2017).
- [13] Naoki Tsukamoto and Yungui Gong, Retrolensing by a charged black hole, *Phys. Rev. D* 95, 064034 (2017).
- [14] K. S. Virbhadra and C. R. Keeton, Time delay and magnification centroid due to gravitational lensing by black holes and naked singularities, *Phys. Rev. D* 77, 124014 (2008).
- [15] Rajibul Shaikh, Pritam Banerjee, Suvankar Paul, Tapobrata Sarkar, Strong gravitational lensing by wormholes, *JCAP* 07, 028 (2019).
- [16] D. Richstone et al., Supermassive Black Holes and the Evolution of Galaxies, *Nature*, A14, 395 (1998).
- [17] A. Ghez, et al., High Proper-Motion Stars in the Vicinity of Sagittarius A*: Evidence for a Supermassive Black Hole at the Center of Our Galaxy, *The Astrophysical Journal*. 509, 678 (1998).
- [18] R. Schödel, et al. A star in a 15.2-year orbit around the black hole at the centre of the Milky Way, *Nature*. 419, 694 (2002).
- [19] supermassive K. Akiyama et al., Event Horizon Telescope Collaboration, First M87 Event Horizon Telescope Results. I. The Shadow of the Supermassive Black Hole, *Astrophys. J.* 875, L1 (2019).
- [20] K. Akiyama et al., Event Horizon Telescope Collaboration, First M87 Event Horizon Telescope Results. V. Physical Origin of the Asymmetric Ring, *Astrophys. J.* 875, L5 (2019).
- [21] K. Akiyama et al. [Event Horizon Telescope Collaboration], First M87 Event Horizon Telescope Results. VI. The Shadow and Mass of the Central Black Hole, *Astrophys. J.* 875, L6 (2019).
- [22] S. V. Iyer and E. C. Hansen, Light's bending angle in the equatorial plane of a Kerr black hole, *Phys. Rev. D* 80, 124023 (2009).
- [23] You-Wei Hsiao, Da-Shin Lee, and Chi-Yong Lin, Equatorial light bending around Kerr-Newman black holes, *Phys. Rev. D*. 101, 064070 (2020).
- [24] J. R. Wilson, Some Magnetic Effects in Stellar Collapse and Accretion, *Ann. N.Y. Acad. Sci.*

- 262, 123 (1975).
- [25] T. Damour, R. Hanni, R. Ruffini, and J. Wilson, Regions of magnetic support of a plasma around a black hole, *Phys. Rev. D* 17, 1518 (1978).
 - [26] Chen-Yu Liu, Da-Shin Lee, and Chi-Yong Lin, Geodesic motion of neutral particles around a Kerr–Newman black hole, *Class. Quantum Grav.* 34 235008 (2017).
 - [27] Chunhua Jiang and Wenbinm Lin, Post-Newtonian light propagation in Kerr–Newman space-time, *Phys. RevD.* 97, 024045 (2018).
 - [28] G. V. Kraniotis, Gravitational lensing and frame dragging of light in the Kerr–Newman and the Kerr–Newman (anti) de Sitter black hole spacetimes, *Gen. Relativ. Gravit.* 46, 1818 (2014).
 - [29] James S. Ulvestad, Goals of the ARISE Space VLBI Mission, *New Astron.Rev.* 43, 531-534 (1999).
 - [30] M. D. Johnson, et al. Universal interferometric signatures of a black hole’s photon ring, *Sci. Adv.* 6, eaaz1310 (2020).
 - [31] Samuel E. Gralla and Alexandru Lupsasca, Null geodesics of the Kerr exterior, *Phys. Rev. D* 101, 044032 (2020).
 - [32] Samuel E. Gralla and Alexandru Lupsasca, Lensing by Kerr black holes, *Phys. Rev. D* 101, 044031 (2020).

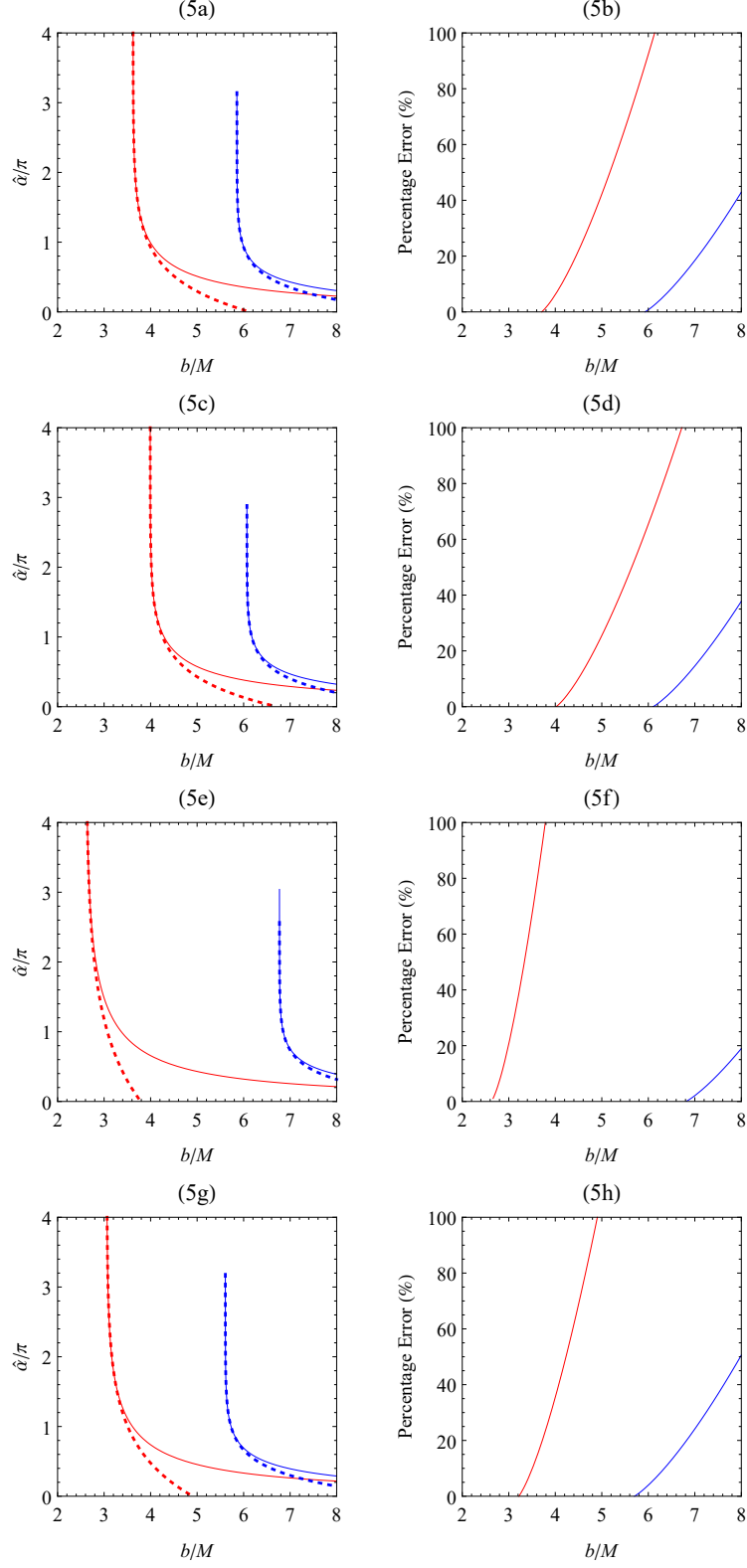


FIG. 5: The SDL deflection angle (dotted lines) and the exact one (solid lines): (5a) $a/M = 0.5$ and $Q/M = 0.6$, (5b) Error between them defined by $(\hat{\alpha}_{exact} - \hat{\alpha})/\hat{\alpha}_{exact} \times 100\%$; (5c) $a/M = 0.5$ and $Q/M = 0.3$, (5d) Error; (5e) $a/M = 0.9$ and $Q/M = 0.3$, (5f) Error; (5g) $a/M = 0.5$ and $Q/M = 0.8$, (5h) Error.